# Polymer Optical Fiber for Angle and Torque Measurements of a Series Elastic Actuator's Spring

Arnaldo G. Leal-Junior, Anselmo Frizera, *Member, IEEE,* Carlos Marques, Manuel R. A. Sánchez, Wilian M. dos Santos, Adriano A. G. Siqueira, *Member, IEEE,* Marcelo V. Segatto and Maria José Pontes

***Abstract*—Series elastic actuators (SEAs) can provide low output impedance, bandwidth close to the human movement and direct measurement of torque through the spring deflection. These advantages enable the application of SEAs in human active orthosis and exoskeletons. However, conventional technologies to measure the spring deflection are bulky, inhibit natural pattern of movement or are sensitive to misalignments. This paper presents the application of polymer optical fiber (POF) as a sensor to measure the spring deflection to overcome some of the issues of conventional technologies, since it is compact, lightweight and have electromagnetic immunity. Furthermore, the spring is employed to validate a torque sensor based on POF stress-optic effects. Results show high linearity of both sensors and mean squared errors below the encoder resolution employed as reference on dynamic measurements.**

***Index Terms*—Polymer optical fiber, Series elastic actuator, torque sensor, angle sensor.**

## I. Introduction

LOCOMOTION plays a crucial role on the capacity to perform activities of daily living, personal functional abilities, and independent development in the community. However, clinical conditions such as stroke, spinal cord injury, Parkinson disease and loss of a member by amputation can affect the human locomotion with varying degrees of severity [1], [2]. To overcome or attenuate human gait disorders, devices such as prostheses [3], exoskeletons [4], and smart walkers [5] have been employed for assistance and rehabilitation purposes.

Lower limb exoskeletons are being used for gait assistance and rehabilitation therapies. Robotic exoskeletons are successfully employed for rehabilitation exercises due to its higher repeatability and the quantitative feedback of the patient recovery [6]. Furthermore, the embedded sensors can also be used for continuous monitoring and evaluation of patient progress with predefined objectives and allowing the customization of treatment with increasing levels of personalization and difficulties. This customization is achieved through the dynamic interaction between the exoskeleton and the patient, which happens with the transition between passive, active-assisted, and active-resisted movements of the robotic device controller [7].

Considering the human safety, it is desirable that the exoskeleton actuators have low output impedance [7]. Otherwise, there is a risk of accident with the patient [7]. Furthermore, the actuators must have a bandwidth close to the one of human movement in order to perform the desired movements of the physiotherapy section. A straightforward manner to achieve these requirements is by placing an elastic element between the load (human limb) and the actuator. This is the series elastic actuator (SEA) principle proposed in [8]. Although the spring placed between the load and the actuator can significantly reduce the system output impedance, it also reduces the system bandwidth [9]. Since the human movement occurs in low frequencies [10], SEAs have been successfully employed as exoskeletons actuators [11], [12], [7], among others.

Another advantage of SEAs is the possibility of estimating the output torque from spring deflection. For this reason, sensors for spring deflection can be employed instead of the torque sensors, which may simplify the actuator instrumentation. However, sensors used to measure these deflections are generally encoders [7] and potentiometers [13] that require mechanical supports precisely assembled due its sensitivity to misalignments. This may result in a less compact system. Additionally, potentiometers may also result in noisy measurements.

Some of the current angle measurement technologies issues may be overcame by optical fiber sensors due to its

This research is financed by CAPES-PGPTA (88887.123920/2014-00 and 88887.095626/2015-01), FAPES (72982608), CNPq (304192/2016-3). C. Marques acknowledges the financial support from FCT through the fellowship SFRH/BPD/109458/2015, program UID/EEA/50008/2013 by the National Funds through the Fundação para a Ciência e a Tecnologia / Ministério da Educação e Ciência, and the European Regional Development Fund under the PT2020 Partnership Agreement.

A. G. Leal Junior, M. A. Sanchéz, A. Frizera, M. J. Pontes and M. V. Segatto are with the Graduate Program of Electrical Engineering of Federal University of Espírito Santo, Vitória, Brazil (e-mail: arnaldo.leal@aluno.ufes.br; frizera@ieee.org; manuel.sanchez@aluno.ufes.br; segatto@ele.ufes.br; mjpontes@ele.ufes.br).

C. Marques is with Instituto de Telecomunicações and Physics Department & I3N, University of Aveiro, Portugal (carlos.marques@ua.pt)

W. M. dos Santos and A. A. G. Siqueira are with Department of Mechanical Engineering, Engineering School of São Carlos, University of São Paulo, Brazil (wilianmds@sc.usp.br, siqueira@sc.usp.br)

compactness, multiplexing capabilities, electromagnetic fields immunity [14]. Regarding the material properties, there are two major types of optical fibers: polymer optical fiber (POF) and glass optical fiber (GOF). POFs may be preferable on angle measurement application due to its higher resistance to impact and vibrations, and higher strain limits that make them more flexible and easy to handle [15].

Among many operation principles for the development of POF sensors, intensity variation is one of the most commonly used principle, due to its easiness of implementation, good cost-quality ratio, and simplicity in signal processing methods [14]. When the fiber is under curvature, there is an attenuation of the fiber output power and this attenuation is related to the angle that the fiber is bent. However, the fiber with no modification presents low sensitivity and linearity with curvature. To improve such parameters, a lateral section is made on the fiber to create a sensitive zone, which increase the sensor sensitivity in over than three orders of magnitude [16].

The POF curvature sensor has been applied as wearable sensor for knee angle measurement [17], lumbar curvature measurements [18], among others. However, the sensor has a saturation trend in angles higher than 90° and the sensor design must consider this behavior. Moreover, polymers are viscoelastic materials and do not have a constant response with stress or strain [19]. Therefore, a viscoelastic behavior compensation should be made in place to obtain a reliable measurement of the sensor. Furthermore, when the fiber is under curvature there is a stress-optic effect, which creates a variation of the fiber refractive index and leads to an attenuation of the POF output power [20].

This paper presents the application of a POF curvature sensor on the elastic element of a SEA. Since small deflections of the spring has to be measured in an effort to estimate the actuator output torque, the sensor has to be carefully placed to obtain a high sensitivity. Another contribution of this paper is a novel torque sensor based on POF stress-optic effect.

This paper is organized as follows. Aiming to describe the POF sensor and analyze the best spot to place it on the spring, Section II discusses the system requirements and operation principle. Section III presents the POF sensor for spring deflection measurements. Section IV depicts the novel torque sensor based on POF. Finally, the final remarks and future works are discussed in Section V.

## II. System Requirements and Operation Principle

### A. POF sensor operation principle

When the fiber is under curvature, there is the attenuation of the power output proportional to the curvature angle [16]. However, a fiber without any modification presents low sensitivity to curvatures [16], which may be increased by performing a lateral section on the fiber creating a sensitive zone. In the case of this work, abrasive removal of material is employed to create such sensitive zone.

The advantage of this technique is the possibility of controlling not only the sensitive zone length and depth, but also the surface roughness of this region [21].

The curvature sensor based on POF presents three power attenuation mechanisms: radiation losses due to macrobends, surface scattering on the sensitive zone, and variation of the refractive index due to the stress-optic effect. Figure 1 shows a top view of the POF under curvature and the attenuation mechanisms are also presented.

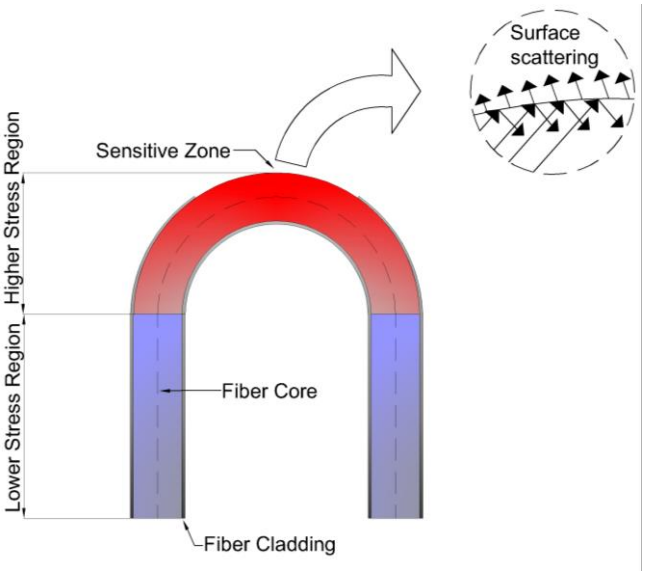


Fig. 1. POF curvature sensor under curvature. There is a region with higher stress due to the stress induced by the bending. The surface scattering and an incident ray propagation is also presented.

The fiber curvature leads to an increase of the reflections in the convex side of the bending and a reduction on the concave side. Since the sensitive zone is on the convex side, there will be more rays escaping if compared with the fiber on the straight position. Therefore, an attenuation of the signal is expected. Moreover, it will increase with the curvature raise. As the bending occurs, angle between the incident ray and the sensitive zone surface increases and creates a variation on the transmission mode. Some higher guided modes are coupled to lower guided modes that increase the surface scattering loss that causes the decrease of the output power, which is another mechanism of attenuation on a POF with sensitive zone [22].

If the light is threated as individual rays, the light source has a constant radiance and only meridional rays are considered. The ratio between input and output power of POF with sensitive zone can be modeled through geometric optics [23], [24]. Equation (1) shows the ratio between input ($P_i$) and output ($P_o$) power of the POF curvature sensor [23].

$$\frac{P_o}{P_i} = \frac{(S_C - S_o)\sin^2(\theta_b)}{S_C \sin^2(\theta_c)}\ , \qquad (1)$$

where $S_C$ is the fiber core cross sectional area, $S_o$ is the maximum area of removed material. The difference between the core cross sectional area and the area of removed material is defined in (2) [23].

$$S_C - S_o = \frac{\pi a^2}{2} + a^2 \arcsin(\frac{a-p}{a}) + (a-p)\sqrt{a^2-(a-p)^2}\,. \quad (2)$$

In this case, $a$ is the fiber core radius and $p$ is the sensitive zone depth.

Referring to (1), $\theta_c$ is the critical angle calculated by the well-known Snell's Law, which varies with the ratio between the core ($n_C$) and cladding ($n_{Cl}$) refractive indexes, and $\theta_b$ is the angle corrected by the fiber bending (3) [23]:

$$\theta_b = \theta_c \sqrt{1 - \frac{2a}{R\theta_c^2}}\,, \quad (3)$$

where $R$ is the curvature radius defined as:

$$R = -\frac{c^2 + 4p^2}{8p}\,, \quad (4)$$

where $c$ is the sensitive zone length [23].

Another effect on the fiber is the variation of the refractive index due to the stress-optic effect [20]. If a pure bending on the z-axis is considered on the region of higher stress on the fiber (see Fig. 1), the variation of the refractive index ($\Delta n_z$) with the stress is defined as [20]:

$$\Delta n_z = \frac{n_C^3 q_{11} \sigma(t)}{2}\,. \quad (5)$$

Referring to (5), $n_C$ is the core refractive index, $q_{11}$ is the fiber stress-optic coefficient, $\sigma(t)$ is the stress, which is time-dependent due to the polymer viscoelasticity [19]. In this equation, the second-order effects due to temperature changes are neglected. Furthermore, the model is valid only for step-index POF, which is also considered transparent, homogenous, and isotropic [20].

### *B. System requirements*

The employed SEA is shown in Fig. 2. It comprises of a customized spring, and a DC motor with an encoder. The transmission of movement is made by a worm gear and the alignment and freedom of movement of the motor axis is guaranteed by an angular contact bearing. Another encoder is positioned on the actuator output axis and the spring deflection is estimated by the difference between the motor encoder and the output axis encoder. Details of the design and construction of this SEA are presented in [7].

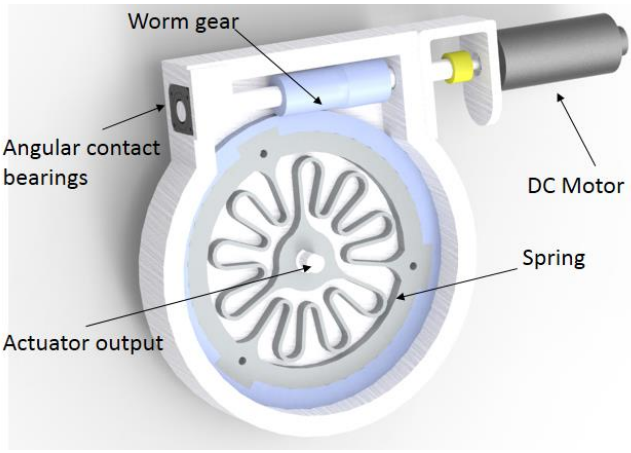


Fig. 2. Rotary Series Elastic Actuator for an active knee orthosis.

However, the goal is obtaining the spring deflection and torque in a robust and straightforward manner. Therefore, it is only necessary to analyze the spring. For this reason, a simpler experimental setup is proposed. The spring with its base and a lever to provide the angular deflection are attached to a support that presents two holes: one at 4° with respect to the lever position when the spring is not under deflection and the other at 10° of the same condition. A lever is employed to position the springs on the predefined angles (see Fig. 3). Furthermore, the encoder E5 series (US digital, USA) is positioned on the spring axis, below the wooden support. This encoder is the reference for the dynamic tests of the POF sensor. Besides its simplicity, this experimental setup also makes the sensor validation easier on both static and dynamic tests.

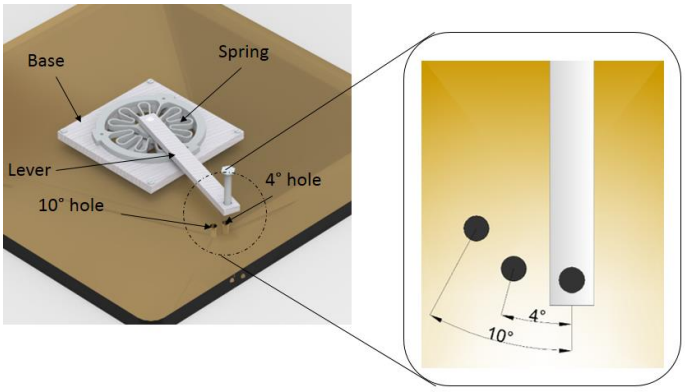


Fig. 3. Experimental setup for the POF sensor validation.

The positioning of the fiber on the spring is of great importance due to the differences of the movement at each portion of the spring. In order to obtain a higher range of movement for the sensor, an analysis of the spring under a predefined stress is made. In this analysis, the spring is fixed and a torque is applied on the center of the spring to simulate the stress that the lever applies on the spring. Figure 4 shows the equivalent strain of the spring when a torque of 15 Nm is applied, which is the maximum torque of the SEA's DC motor when the safety factor is considered [7]. In Fig. 4, the points *a* and *b* present higher relative movement and low equivalent

strain. Therefore, these points are more suitable for the POF sensor position, since there is more range of movement of the sensor and the low equivalent strain, in this region, prevents the fiber rupture and plastic deformation.

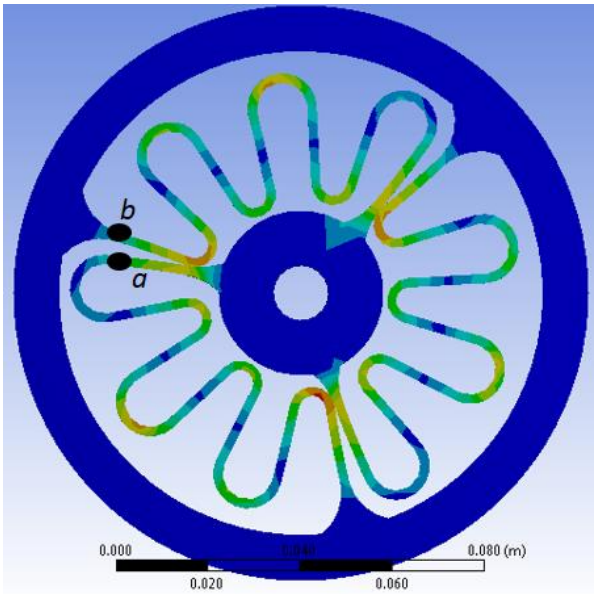


Fig. 4. Equivalent strain of the spring submitted to a 15 Nm torque. The points ***a*** and ***b*** are more suitable for the POF sensor positioning.

The POF sensor has to be positioned perpendicular to the face of the spring shown in Fig. 4. Otherwise, it will interfere on the spring extension movement due to the fiber strain and can slip on the compression movement. Both in extension and compression of the spring, the effects of the sensor mounted on the spring surface will cause a decrease of the sensor sensitivity. Supports for the optical fiber sensor were made to enable the fiber positioning without inhibit the spring movement. These supports are placed on the points ***a*** and ***b*** of the spring presented in Fig. 4. A schematic drawing of the spring with the POF sensor is presented in Fig. 5 (a), whereas, a photograph of the spring with the 3D printed supports and the optical fiber sensor is shown in Fig. 5 (b).

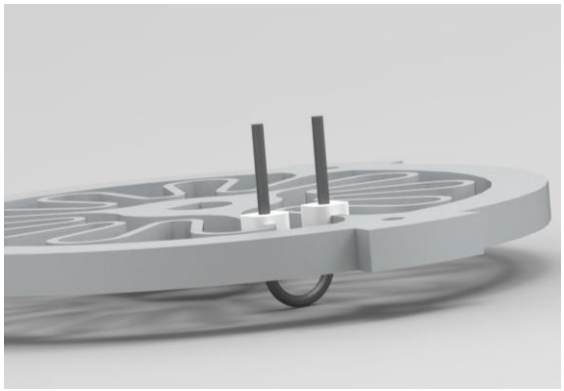

(a)

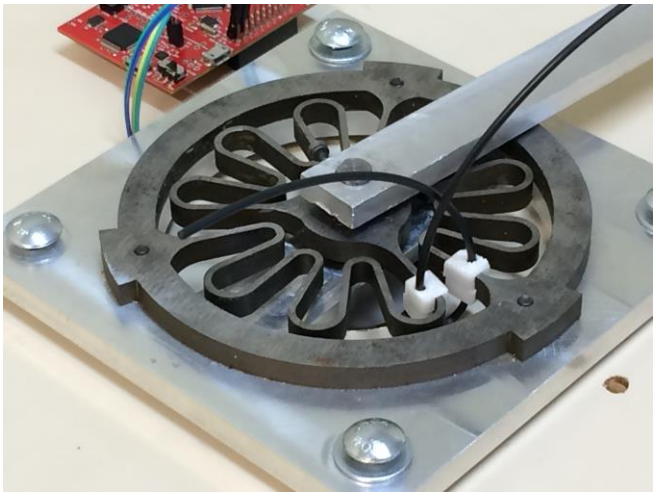

(b)

Fig. 5. (a) Schematic drawing of the POF sensor attached on the spring and (b) Photograph of the spring with the 3D printed supports for the POF sensor positioning.

## III. Method for Angular Deflection Measurement

Applications of POF curvature sensors involve a calibration phase on static or quasi-static conditions prior to the application of the sensor on dynamic measurements [17]. In this case, the first measurements are made on static conditions, which are on 0°, 4° and 10°. The sensor response at each of these angles are acquired and a calibration curve is obtained.

The lever is connected to the spring output as presented in Fig. 3. For this reason, the angular movement of the lever is directly transmitted to the spring. Therefore, the characterization of the angular deflection is made by positioning the lever on the holes with an angular displacement with respect to the lever initial position of 4° and 10° (see Fig. 3) for about 150 seconds at each angle. A laser with 3 mW @650 nm is connected to one end of the fiber. Whereas, the other end of the fiber is connected to a photodiode with a transimpedance amplifier circuit. The acquisition frequency is 200 Hz. Since the POF sensor can present measurement errors with the variation of temperature and humidity [21], all tests are made without the variation of these parameters. In addition, another POF, connected to the same light source, is positioned close to the spring without any strain applied on it for temperature and humidity monitoring.

POFs are viscoelastic materials, which present a time-varying relationship of stress and strain due to molecular rearrangement. Towards enabling a more real and complete characterization of this response and to obtain a compensation of the POF's viscoelastic response, the authors propose and implement a procedure similar to the creep recovery test [25]. The creep recovery is employed to characterize the viscoelastic parameters, which comprises of apply a constant force on the fiber and measure its deformation. If the material is perfectly elastic, a constant stress input will result in a constant strain output. For a viscoelastic material, there is an exponential decay of the strain response with time. The optical response of the fiber when the spring is deflected in 10° has the same behavior of the creep recovery experiment response,

This article has been accepted for publication in a future issue of this journal, but has not been fully edited. Content may change prior to final publication. Citation information: DOI 10.1109/JLT.2017.2789192, Journal of Lightwave Technology



where there is a constant force and the elongation varies due to the polymer viscoelastic behavior until it reaches its relaxation time, which is also similar to the one presented in [19]. Figure 6 shows the elongation of the fiber under a unitary (normalized) stress, where it can be seen that the normalized elongation presents an initial amplitude higher than the one of the stress (unitary), followed by a decay of the fiber elongation due to the polymer relaxation.

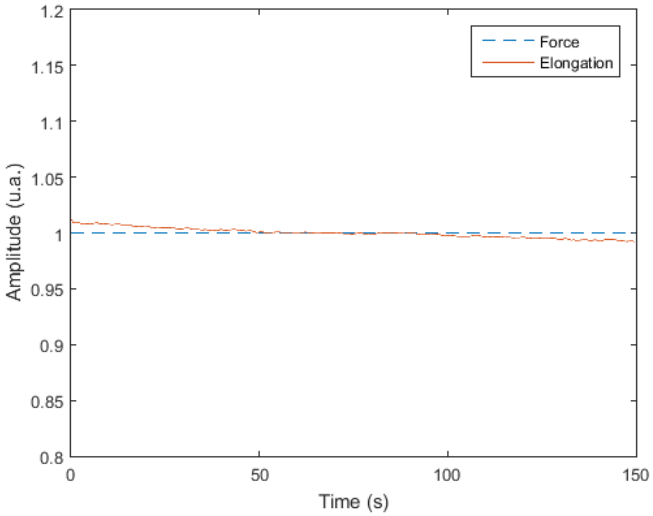


Fig. 6. Fiber response with a constant stress input.

The viscoelastic response may be modeled with the Maxwell's viscoelastic model [25]. In this model, the viscoelastic response is approximated as a system with a spring and a dashpot connected in series. The spring represents the elastic component of the material response. Whereas, the dashpot is related to the material viscous response. Applying this principle to the POF curvature sensor response, it is possible to disconnect the time-varying and the static components of the response. By doing so, an equation relating the dynamic response ( $P(t)$ ) and the static response ( $P_0$ ) is obtained by:

$$P(t) = P_0 \exp(-\frac{t}{\tau}), \quad (6)$$

where $t$ is the time and $\tau$ is the polymer time constant, which can be obtained by an exponential fit of the creep experiment response. Furthermore, the static response of the sensor can be isolated on (6) to obtain an expression to compensate the viscoelastic effects of the sensor. Figure 7 presents the compensated and uncompensated responses for the viscoelastic effect on the sensor response of the static characterization with 10° deflection of the spring. The stress on a fiber generates a variation of the signal. Therefore, it is expected that the optical response of the sensor without the time-varying component will be inverse in modulus when compared to the one obtained in creep recovery.

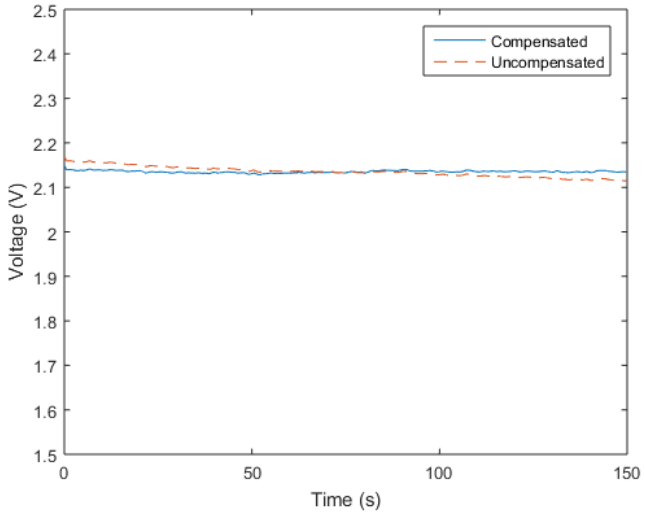


Fig. 7. Comparison between compensated and uncompensated responses of the POF sensor when the spring is deflected in 10°.

The compensated responses for the 10° and 4° deflections were 2.14 V and 2.01 V, respectively. In addition, the response when no deflection is applied on the spring is 1.92 V. These responses are related to the spring angles through a linear regression. The calibration curve and correlation coefficient are presented in Fig. 8.

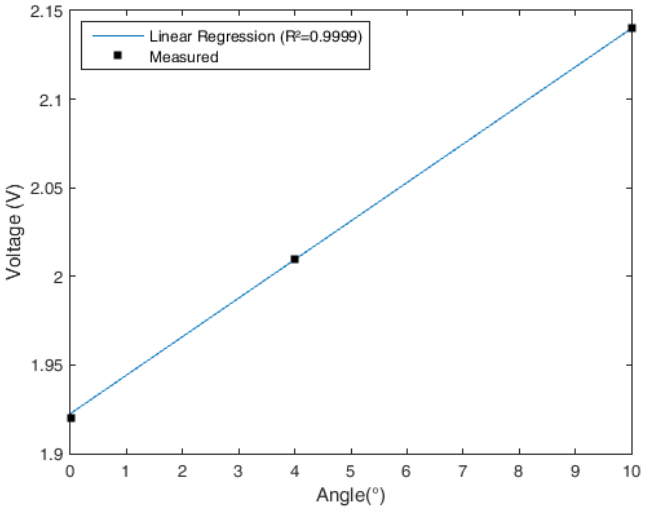


Fig. 8. Calibration curve of the POF curvature sensor.

The dynamic response of the sensor is evaluated on sequential compression cycles. The tests comprise of loading and unloading the lever for about 3.5 seconds. Figure 9 shows the results for the POF sensor and the encoder measurements, which are not continuous for a better visualization of the POF response.

This article has been accepted for publication in a future issue of this journal, but has not been fully edited. Content may change prior to final publication. Citation information: DOI 10.1109/JLT.2017.2789192, Journal of Lightwave Technology



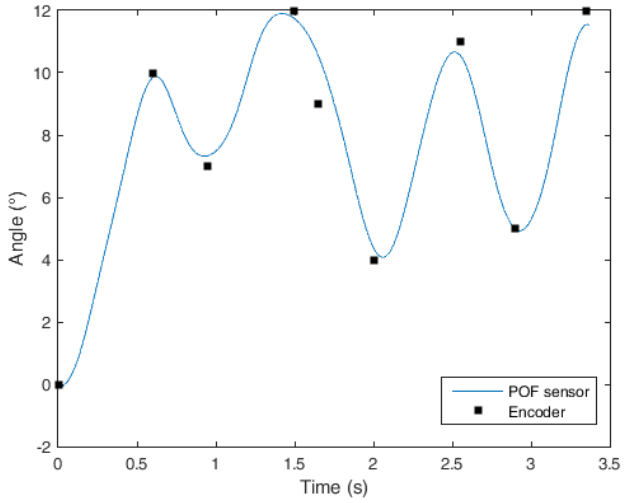


Fig. 9. POF curvature sensor response for successive loading/unloading cycles and encoder measurements.

The root mean squared error (RMSE) is calculated between the POF sensor and the encoder. For this test, the RMSE is about 0.57°. However, it should be noted that the two systems present different behaviors on the dynamic tests. The encoder response is in steps of 0.3°. Whereas, the POF sensor presents almost continuous response with a resolution of 0.1° when considering the 8-bit ADC. For this reason, it may be an angle that is below the encoder resolution, but it is within the POF sensor resolution that will be calculated as an error of the POF sensor. Therefore, this RMSE may be lower if a higher resolution system is employed as reference. Nevertheless, the POF sensor presented errors lower than 4% when considering the entire range of the test.

## IV. Proposal and Validation of Novel Technique for Torque Measurement

Despite the good accuracy of the POF curvature sensor, it generally has a saturation trend of its response in angles higher than 90°. However, in this case, the initial position of the sensor is already on a 180° bend (see Fig. 5) and the sensor shows a linear behavior. One reason for this behavior may be a trade-off between the radiation losses due to the curvature and the attenuation generated by the refractive index variation that the stress-optic effect causes. In order to verify this assumption, the POF sensor is bent in angles from 0 to 100°. Since the fiber is at straight position and the distance between the supports on both ends of the POF is 40 mm, the stress on the fiber is lower than in the condition of the spring deflection measurements presented in Fig. 5. In such conditions, the fiber is at 180° and the distance between the supports is about 9 mm, which leads to a higher stress on the fiber [21]. Figure 10 shows the response when the fiber is under a curvature of 0° to 100° with constant velocity of 0.0561 rad/s.

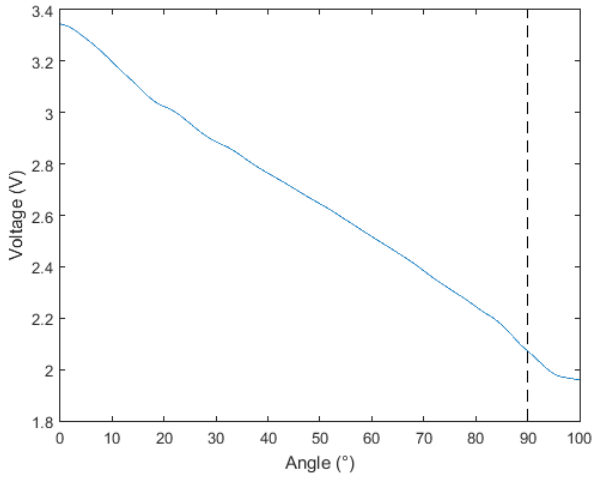


Fig. 10. POF sensor response in 0 to 100° bend with angular velocity 0.0561 rad/s. The dashed line represents the angle of 90°.

Referring to Fig. 10 there is a clearly saturation trend when the angle is higher than 90°. However, in Fig. 8 the sensor has a response almost linear with the fiber under curvature angles of 180° of the POF positioning on the spring (see Fig. 5) plus the 10° of the spring deflection. The assumption of the difference between the sensor behavior in Fig. 8 and Fig. 10 is a higher influence of the stress-optic effect on the sensor response when it is submitted to higher stress. Since there is a relation between the stress and the refractive index variation, it is expected that if the stress-optical effect is dominant, the sensor response will show high attenuation even if it is submitted to angles above 90°.

Another evidence for the assumption of stress-optical effect dominance is the static tests made on Section III. In these tests, the sensor presents the characteristic response of viscoelastic materials on creep recovery or stress relaxation tests [25]. For obtaining the differences between static tests of the fiber placed on the spring (initial angle of 180°) and on the straight position, a static test is performed with the fiber on the straight position. In this test, the fiber is bent from straight position (0°) until 100° on steps of 5° and it remains at each position for 10 seconds. The results are shown in Fig. 11, which can be seen that the response does not show the characteristic response of viscoelastic material. Since when the fiber is at the straight position the stress-optical effect is not dominant, there is not an exponential decay of the POF response at each angle, which represent different levels of stress on the fiber. In other words, if the curvature angle increases, the stress over the fiber also increases. Therefore, Fig. 11 shows reinforce the assumption that the stress-optical effect is dominant on the response of the POF sensor placed on the torsional spring.

This article has been accepted for publication in a future issue of this journal, but has not been fully edited. Content may change prior to final publication. Citation information: DOI 10.1109/JLT.2017.2789192, Journal of Lightwave Technology



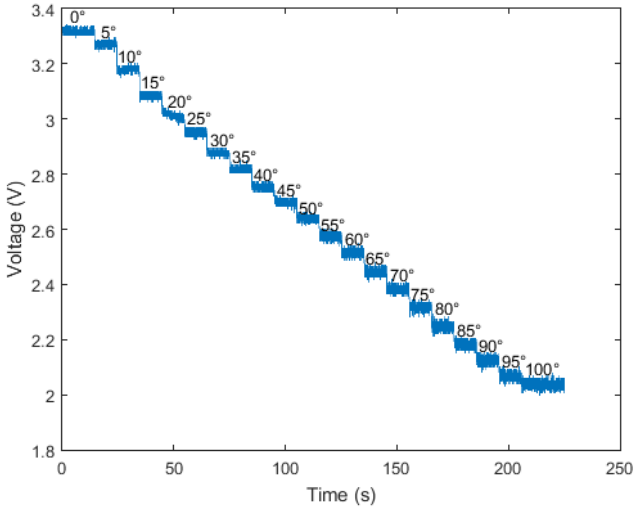


Fig. 11. POF sensor response on static tests with curvature angle between 0° and 100°.

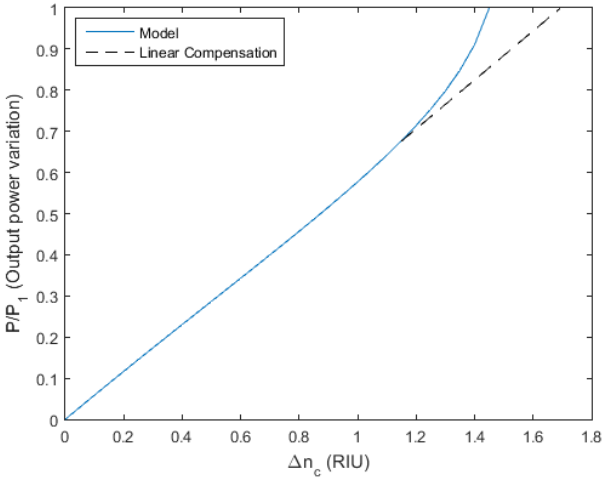


Fig. 12. POF sensor output power variation with different refractive indexes and the linear compensation for refractive indexes higher than 1.3 RIU.

Based on the evidences here shown, the assumption for the POF torque sensor is that since the fiber is initially bended in 180°, all the attenuation of the optical power is due to the variation of the refractive index caused by the stress-optical effect. Furthermore, as assumed for the deflection in Section III, all the torque generated by the spring deflection is directly transmitted to the fiber. For this reason, different refractive indexes are applied on the equation of the sensor attenuation (see (1)) to obtain the relation between the output power attenuation and the refractive index variation. The POF sensor properties are presented in Table 1. To enhance the signal visualization, the output power signal is normalized with respect to the first signal (when the refractive index variation is 0). Figure 12 shows the relation between the sensor output variations with the refractive index variation ( $\Delta n_c$ ).

TABLE I
POF SENSOR PROPERTIES

| Parameter | Value | Unit |
|---|---|---|
| $a$ | 0.49 | mm |
| $p$ | 0.60 | mm |
| $c$ | 12.48 | mm |
| $n_c$ | 1.492 | - |
| $n_{cl}$ | 1.417 | - |
| $q_{11}$ | $10^{-11}$ | $m^2/N$ |

The output power variation with the refractive index changes is almost linear. However, the relation does not have a linear behavior when the refractive index variation is higher than 1.3. Such relation is obtained applying (5) under the consideration that all power attenuation is due to the stress-optic effect, and it may lead to errors on the torque measurement. In order to compensate the effect of this nonlinearity on the torque measurement, a linear approximation of the curve relating the refractive index variation and the output power is made for refractive indexes higher than 1.3 (see Fig. 12).

The variation of the core refractive index due to the stress-optic effect is given by (5). Furthermore, as shown in Section III, the time-varying component of the sensor viscoelastic response can be isolated from the static component through (6). Since the main assumption here is that all the signal attenuation is due to the stress-optical effect, (6) can be applied for the stress response of the sensor shown in (5). If pure bending stress is considered, the static stress ( $\sigma_0$ ) can be calculated as:

$$\sigma_0 = \frac{Tx}{I}, \tag{7}$$

where $T$ is the torque, $x$ is the perpendicular distance between the bending axis and the neutral line (fiber center dashed line of Fig. 1), and $I$ is the moment of inertia around the neutral axis. Applying the assumption that all the output signal variation is due to the stress-optical effect, (6) can be rewritten with stress terms instead of optical power terms. By taking the compensated response and substituting (7) in the (5), the torque equation for the POF torque sensor is obtained as:

$$T = \frac{\Delta n_c 2I}{n_c^{\,3} q_{11} x}. \tag{8}$$

Since the fiber cross sectional area is circular, the moment of inertia depends only on the POF total diameter, which is the 0.98 mm of the core plus the 20 µm thickness of the cladding and the 1.2 mm of the jacket that totalizes the diameter of 2.2 mm of the POF employed. The distance between the bending axis and the neutral line is the length indicated as "higher stress region" in Fig. 1. The length of this region is about 3.5 mm. Although the value of this distance can change with the bending angle, this variation is not high in this case due to the lower angles of spring deflection, which is lower than 12° (see Fig. 9) and the lower curvature radius of the fiber in this case. Therefore, the distance between the bending axis and the neutral line, $x$, is considered constant. In order to get the refractive index variation, the range of variation of this parameter with the output power can be approximated through linear regressions. Equation (9) shows the linear regression for the result presented in Fig. 12. This equation gives the estimated refractive index ( $n_{est}$ ) with a certain output power variation.

$$n_{est} = 1.571\frac{P}{P_1} + 0.04474 \qquad (9)$$

The difference between the estimated refractive index when the output power ratio is 1 (1.616, see (9)) and the estimated refractive index for a certain output power ratio is the refractive index variation.

The torque curve is compared with the measurements made on the spring. Since the spring presented high linearity on both extension and compression movements [7], the torque on the spring under compression is the product between the spring constant for compression, which is 92 Nm/rad, and the spring deflection angle. When the deflection angle is 4°, the spring torque is 6.42 Nm. Whereas, the torque estimated by the sensor based on POF is 6.78 Nm, this difference represents an error of 5%. However, this error is reduced as the spring deflection angle increases. When the spring angle is 10°, the torque is 16.05 Nm and the POF torque sensor estimates a torque of 16.57 Nm, which is an error of 3.2%.

The POF torque sensor is also validated in dynamic measurements. The test result presented in Section III is evaluated with respect to the torque by means of the product between the spring deflection measured by the encoder and the spring constant. Figure 13 presents the test results and the torques estimated by the torque sensor. The RMSE is also calculated in this case. The error between the POF sensor and the encoder for the torque estimations is 0.33 Nm. The errors that can be present due to the encoder resolution discussed in Section III, are also presented in this test. Although the deflection range is low, the assumption of constant moment of inertia and constant perpendicular distance between the bending axis and the neutral line also can lead to minor deviations on the torque estimation. For this reason, the error of the torque sensor is higher than the one of the curvature sensor. The comparison between the RMSE for the torque and the angle is made by calculating the percentage contribution of the RMSE on the total range of the test, which means to calculate a ratio between the RMSE and the test range. In this way, the error percentage contribution of the torque sensor is 5.7%. Whereas, the percentage contribution of the curvature sensor is 4.7%. The error of the torque sensor may be further reduced if the variation of the distance between the bending axis and the neutral line is considered for the different deflection angles on the spring. Nevertheless, Fig. 13 also shows the comparison between the proposed technique for torque measurement with POF sensors and the POF curvature sensor with the application of the spring constant to estimate the torque, an alternative manner to determine torque on a torsional spring. Regarding the sensor resolution, the estimated value for the torque measurement is about 0.15 Nm, which provides a higher resolution than the encoder (about 0.5 Nm). In addition, the sensor errors for the torque measurements is lower than 5%, which may indicate high precision of the proposed POF sensor.

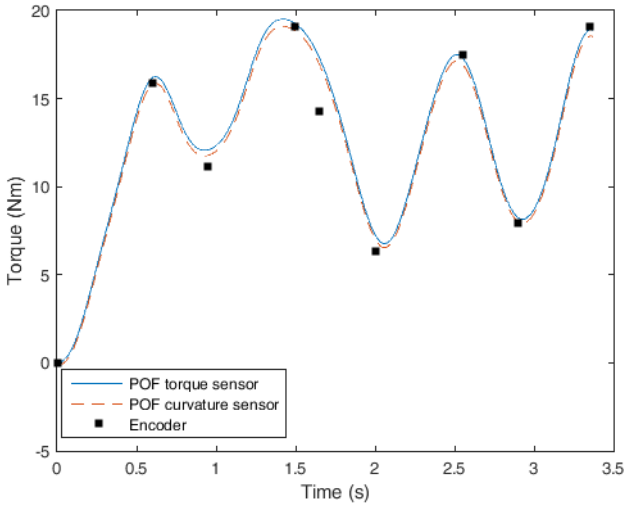


Fig. 13. Torque estimated by the POF torque sensor for successive loading/unloading cycles and torque estimated by the encoder and POF curvature sensor with the application of the spring constant.

## V. Conclusions

This paper presents the application of POF sensors on the spring of a rotary SEA for active knee orthosis. Two different methods were developed for obtaining spring's deflection and torque.

The spring deflection was obtained by means of the correlation line between the sensor output voltage and the spring deflection. The correlation equation is obtained on the calibration procedure, which comprises of positioning the spring on predefined angular positions and acquire the sensor output power in each position. Considering that POFs present viscoelastic response with the consequent time-varying component on its stress or strain response, a reliable deflection response is obtained through the viscoelastic effects compensation made with creep recovery or stress relaxation experiments. This compensation successfully isolates the static response from the time-varying response.

Since the sensor response presented the effect of a viscoelastic material under stress and the sensor does not present the characteristic saturation trend in angles higher than 90°, it was made the assumption that all the variation of the output power is due to the variation of the refractive index induced by the stress-optical effect. This assumption enables the application of the POF to measure the torque on the spring.

The proposed torque sensor presents lower errors when the refractive index is smaller than 1.3. However, there is a discontinuity of the model when the refractive index is higher than 1.3. A linear compensation to correct/suppress this effect was proposed and the error remains below 5.7%. Although this error is higher if no compensation is applied, the compensation technique may be enhanced by considering the neutral line distance variation with the spring deflection angle, which is theme of future works.

Another future work includes the investigation of the trade-off between the attenuation mechanisms of the POF sensor in angles lower than 90°. In this way, it may be possible to measure angle and torque simultaneously, which has potential applications as wearable sensors for human kinematics and kinetics assessment, increase the compactness of exoskeleton instrumentation and as sensors for soft robotics.

## REFERENCES

[1] A. L. Hsu, P. F. Tang, M. H. Jan, “Analysis of impairments influencing gait velocity and asymmetry of hemiplegic patients after mild to moderate stroke,” Archives of Medicine and Rehabilitation, vol. 84, no. 8, pp.1185-1193, 2003.

[2] I. Tien, S. D. Glaser, M. J. Aminoff, “Characterization of gait abnormalities in Parkinson’s disease using a wireless inertial sensor system,” 2010 Annual International Conference of IEEE Engineering in Medicine and Biology Society, 31 Aug - 04 Sep 2010, Buenos Aires – Argentina, pp. 3353-3356, 2010.

[3] K. H. Ha, H. A. Varol, and M. Goldfarb, “Volitional control of a prosthetic knee using surface electromyography,” IEEE Trans. Biomed. Eng., vol. 58, no. 1, pp. 144–151, 2011.

[4] A. J. del Ama Espinosa, “Hybrid walking therapy with fatigue management for spinal cord injured individuals,” Phd. Thesis Universidad Carlos III de Madri, 2013.

[5] C. Cifuentes, A. Frizera, “Human-Robot Interaction strategies for walked-assisted locomotion.” Springer Tracts in Advanced Robots, 2016.

[6] G. Kwakkel, B. Kollen, and H. Krebs, “Effects of robot-assisted therapy on upper limb recovery after stroke: a systematic review,” Neurorehabil. Neural Repair, 2007.

[7] W. M. dos Santos, G. A. P. Caurin, and A. A. G. Siqueira, “Design and control of an active knee orthosis driven by a rotary Series Elastic Actuator,” Control Eng. Pract., vol. 58, pp. 307–318, 2017.

[8] G. A. Pratt and M. M. Williamson, “Series elastic actuators,” IEEE/RSJ International Conference on Intelligent Robots and Systems. “Human Robot Interaction and Cooperative Robots,” vol. 1, no. 1524. pp. 399–406, 1995.

[9] D. W. Robinson, “Design and analysis of series elasticity in closed-loop actuator force control,” Mech. Eng., p. 123, 2000.

[10] C. Kirtley, “Clinical gait analysis: Theory and practice.” Philadelphia, PA: Elsevier Churchill Livingstone, 2006.

[11] K. Kong, J. Bae, M. Tomizuka, “Control of rotary series elastic actuator for ideal force mode actuation in human robot interaction applications,” IEEE/ASME Transactions on Mechatronics, vol. 14, no. 1, pp. 105–118, 2009.

[12] C. Lagoda, A. Schouten, A. Stienen, E. Hekman, H. van der Kooij, “Design of an electric series elastic actuated joint for robotic gait rehabilitation training,” Proceedings of 3rd IEEE RAS and EMBS international conference on biomedical robotics and biomechatronics (pp. 21–26), Tokyo, Japan, 2010.

[13] A. G. Leal Junior, R. Andrade, A. Bento Filho, “Series Elastic Actuator: Design, Analysis and Comparison,” Recent Advances in Robotic Systems, InTech, DOI: 10.5772/63573, 2016.

[14] L. Bilro, N. Alberto, J. L. Pinto, and R. Nogueira, “Optical sensors based on plastic fibers,” Sensors (Switzerland), vol. 12, no. 9, pp. 12184–12207, 2012.

[15] K. Peters, “Polymer optical fiber sensors—a review,” Smart Mater. Struct., vol. 20, no. 1, p. 13002, 2011.

[16] Y. Fu, H. Di, and R. Liu, “Light intensity modulation fiber-optic sensor for curvature measurement,” Opt. Laser Technol., vol. 42, no. 4, pp. 594–599, 2010.

[17] L. Bilro, J. G. Oliveira, J. L. Pinto, and R. N. Nogueira, “A reliable low-cost wireless and wearable gait monitoring system based on a plastic optical fibre sensor,” Meas. Sci. Technol., vol. 22, no. 4, p. 45801, 2011.

[18] J. M. Williams, I. Haq, and R. Y. Lee, “Dynamic measurement of lumbar curvature using fibre-optic sensors,” Med. Eng. Phys., vol. 32, no. 9, pp. 1043–1049, 2010.

[19] A. Stefani, S. Andresen, W. Yuan, and O. Bang, “Dynamic characterization of polymer optical fibers,” IEEE Sens. J., vol. 12, no. 10, pp. 3047–3053, 2012.

[20] J. Zubia, J. Arrue, and A. Mendioroz, “Theoretical Analysis of the Torsion-Induced Optical Effect in a Plastic Optical Fiber,” Opt. Fiber Technol., vol. 3, no. 2, pp. 162–167, 1997.

[21] A. G. Leal-Junior, A. Frizera, and M. José Pontes, “Sensitive zone parameters and curvature radius evaluation for polymer optical fiber curvature sensors,” *Opt. Laser Technol.*, vol. 100, pp. 272–281, 2018.

[22] R. Liu, Z. Fu, Y. Zhao, Q. Cao, and S. Wang, “Operation principle of a bend enhanced curvature optical fiber sensor,” IEEE Int. Conf. Intell. Robot. Syst., pp. 1966–1971, 2006.

[23] L. Bilro, N. J. Alberto, L. M. Sá, J. De Lemos Pinto, and R. Nogueira, “Analytical analysis of side-polished plastic optical fiber as curvature and refractive index sensor,” J. Light. Technol., vol. 29, no. 6, pp. 864–870, 2011.

[24] M. Kovacevic, A. Djordjevich, D. Nikezic, “Analytical optimization of optical fiber curvature gauges,” IEEE Sensors Journal, vol. 8, no.3, pp. 227-232, 2008 [doi: 10.1109/jsen.2007.913139].

[25] R. Lakes, “Viscoelastic Materials,” Cambridge University Press, First Edition, 2009.